A Finite Element Model of the face including an orthotropic skin model under *in vivo* tension

Cormac Flynn (Corresponding Author)

Ian Stavness

John Lloyd

Sidney Fels

Word Count: 4053

Abstract

Computer models of the human face have the potential to be used as powerful tools in surgery simulation and animation development applications. While existing models accurately represent various anatomical features of the face, the representation of the skin and soft tissues are very simplified. A computer model of the face is proposed where the skin is represented by an orthotropic hyperelastic constitutive model. The *in vivo* tension inherent in skin is also represented in the model. The model was tested by simulating several facial expressions by activating appropriate orofacial and jaw muscles. Previous experiments calculated the change in orientation of the long axis of elliptical wounds on patients' faces for wide opening of the mouth and an open-mouth smile (both 30^{o}).These results were compared to the average change of maximum principal stress direction in the skin calculated in the face model for wide opening of the mouth (18^{o}) and an open-mouth smile (25^{o}). The displacements of landmarks on the face for four facial expressions were compared with experimental measurements in the literature. The corner of the mouth in the model experienced the largest displacement for each facial expression (~11 mm to 14 mm). The simulated landmark displacements were within a standard deviation of the measured displacements. Increasing the skin stiffness and skin tension generally resulted in a reduction of landmark displacements upon facial expression.

Keywords:

Face model; Constitutive model; *In vivo* tension; Anisotropy; Expressions;

Introduction

Computer models of the human face have a broad range of applications in the biomedical, forensic, and animation fields (Zhang et al. 2004, Claes et al. 2010, Mollemans et al. 2007). In

biomedical engineering, they can be used in the analysis of physiological conditions, such as face dismorphosis (Kim et al. 2010). Surgical procedures, such as mandible reconstruction, can result in severe facial scarring after healing. As well as being aesthetically unpleasing for the patient, this scarring can lead to dysphagia and difficulties in mastication (Virgin et al. 2010). Facial computer models could help identify superior surgical techniques to minimize post-operative scarring and help regain function and thus improve the quality-of-life of the patient (Hannam 2011). For victims of severe burn injuries, face models could also be used to develop realistic facial prostheses, which mimic the wrinkling and deformation of real skin (Bellamy et al. 2003).

While recent models accurately represent anatomical features such as the skull, jaw, and soft tissues, they also make several assumptions with respect to facial skin. Almost all facial models in the literature assume skin to be an isotropic, elastic material (Barbarino et al. 2009, Nazari et al. 2011, Nazari et al. 2010) and some assume it to have a linear stress-strain curve (Beldie et al. 2010, Gladilin et al. 2004). Several models assume skin to be single-layer and ignore the individual contributions of the dermis and hypodermis (Chabanas et al. 2003). No facial model considers the relaxed skin tension lines (RSTLs) inherent in living skin, a parameter that is important in wrinkling phenomena and an influential parameter in the orientation of surgical incisions (Borges 1984). Skin is a complex anisotropic, multi-layer material under tension and, so to make meaningful predictions of surgical outcome, facial skin models must take these characteristics into account (Wilkes et al. 1973).

There is a need in surgical simulations for a numerical model of the face, which includes the anisotropic, multi-layer characteristics of skin as well as the *in vivo* tension. It is proposed that including these characteristics will result in a model, which can better simulate deformations and phenomena observed in *in vivo* facial skin experiments. This paper presents a finite element

model of the face, which includes an anisotropic, multi-layer representation of skin under tension. Validation of the model involves simulating different facial expressions and comparing model results to experimental data in the literature. The experimental data consist of *in vivo* tension field orientations and facial landmark displacements for different expressions. The effect of changing the mechanical properties of the skin (in accordance to what is observed in aging skin) on landmark displacements is investigated.

1 Material and Methods

Finite Element Face Model

The model is embedded within Artisynth (www.artisynth.org), an open source biomechanical modelling platform developed at the University of British Columbia (Stavness et al. 2011).

The finite element model consists of several parts including a cranium and maxilla component; a jaw-hyoid component, which has been used to simulate free-jaw movements and chewing (Stavness et al. 2011); and a soft-tissue component representing the skin and hypodermal layers (Figure 1). All the bony components are modelled as rigid bodies. The jaw muscles consist of point-to-point Hill-type actuators.

The soft tissue finite element mesh is similar to that presented in Nazari et al. (2011), except the inner and outer surface of the present mesh correspond to inner and outer surfaces of CT data from an adult male (Bucki et al. 2010). The mesh consists of 6342 elements and 8720 nodes, using mostly linear hexahedral elements and the remainder being linear wedge elements. There are three layers of elements throughout the mesh. The outside layer represents the epidermis and dermis, while the middle and inside layers represent the hypodermal soft tissues. The thickness of the outside layer is about 1.5 mm, which is representative of skin thicknesses

measured for the face (Barbarino et al. 2011, Ha et al. 2005, Lee and Hwang 2002). The layers representing the hypodermal layers range in total from about 4 mm to 11 mm, which are within ranges reported in the literature (Barbarino et al. 2011, Domaracki and Stephan 2006, Manheim et al. 2000). Doubling the mesh density resulted in no significant difference in the results.

Ten orofacial muscles are represented in the face model (Figure 2 and Table 3). The elements of the soft tissue mesh that are in the region of a facial muscle are assigned a fibre direction corresponding to the principal direction of the facial muscle at that point. Elements containing a muscle fibre are assigned the properties of the muscle, which contains passive and active components. The total Cauchy stress equation in the muscle fibre is based on Weiss et al. (1996) (Equation 4 in the Appendix). The passive force in the muscle fibre is based on work by Blemker et al. (2005) (see Equation 7 in the Appendix).

The cranium, maxilla, and hyoid are fixed in space, along with the appropriate end-points of the jaw muscles. The zygomatic ligaments are represented by fixing all degrees-of-freedom of soft tissue nodes that are in the region where these ligaments attach to the maxilla (Furnas 1989). Likewise, the mandibular ligaments are represented by attaching the appropriate soft tissue nodes to the mandible (Furnas 1989). All nodes along the edge of the domain, where representation of the soft tissue ends, are fixed in all degrees-of-freedom. It is assumed that these nodes are sufficiently removed from the area of interest that they do not have an effect on the analyses. Contact between the inside surface of the soft tissue and bony structures is modelled, along with contact between upper and lower lip surfaces. Gravity effects, with an acceleration equal to 9.8 ms^{-2}, are included in the model.

Soft Tissue Constitutive Equations

The hypodermis of the soft tissue model is represented by a Mooney-Rivlin constitutive

equation, where the strain energy is given by

$$W = C_{10}\left(\tilde{I}_1 - 3\right) + C_{20}\left(\tilde{I}_1 - 3\right)^2 + \frac{\kappa}{2}\left(\ln J\right)^2 \tag{1}$$

C_{10}, C_{20}, and κ are material parameters; $\tilde{I}_1 = trace\left(\tilde{\mathbf{B}}\right)$ is the first invariant of the distortional part of the left Cauchy-Green tensor, $\tilde{\mathbf{B}} = \tilde{\mathbf{F}}\tilde{\mathbf{F}}^{\mathrm{T}}$, where $\tilde{\mathbf{F}} = J^{-1/3}\mathbf{F}$ is the distortional part of the deformation gradient **F**; $J = \det\left(\mathbf{F}\right)$ is a measure of the pure volume change. The material parameters used were taken from recent *in vivo* suction tests on facial skin (Barbarino et al. 2011) (see Table 2).

A frame-invariant version of the Fung constitutive equation is used to represent the epidermis and dermis layers (Ateshian and Costa 2009). The strain energy function is given by

$$W = \frac{1}{2}c\left(e^{Q} - 1\right) + \frac{\kappa}{2}\left(\ln J\right)^2 \tag{2}$$

where c is a material parameter and Q is given by

$$Q = c^{-1}\sum_{a=1}^{3}\left[2\mu_a \mathbf{A}_a^0 : \tilde{\mathbf{E}}^2 + \sum_{b=1}^{3}\lambda_{ab}\left(\mathbf{A}_a^0 : \tilde{\mathbf{E}}\right)\left(\mathbf{A}_b^0 : \tilde{\mathbf{E}}\right)\right] \tag{3}$$

where μ_a and λ_{ab} are material parameters (note that $\lambda_{ab} = \lambda_{ba}$). $\tilde{\mathbf{E}} = \frac{1}{2}\left(\tilde{\mathbf{F}}^{\mathrm{T}}\tilde{\mathbf{F}} - \mathbf{I}\right)$ is the distortional part of the Green-Lagrange strain tensor. $\mathbf{A}_a^0 = \mathbf{a}_a^0 \otimes \mathbf{a}_a^0$, where $\mathbf{a}_a^0$ defines an initial direction of a material axis a. In order to specify $\mathbf{a}_a^0$, a Matlab script was written whereby the RSTLs were traced out on the surface of the face model with a mouse and using Borges (1984) as a reference (Figure 3(a)). An element in the outer layer of the soft tissue mesh was then assigned the direction of the RSTL segment closest to it. The vector representing this RSTL segment was then projected onto the external surface of the element (Figure 3(b)). This vector was assigned to

$\mathbf{a}_1^0$ for this element. $\mathbf{a}_2^0$ was specified as the normal to the external surface of the element. $\mathbf{a}_3^0$ was determined from the cross product of $\mathbf{a}_1^0$ and $\mathbf{a}_2^0$.

The material parameters for the skin (c, μ_a, λ_{ab}) were based on *in vivo* experiments in which a micro-robotic device applied a rich set of deformations to human forearm skin (Flynn et al. 2011). Using the material parameters determined by Flynn et al. (2011), simulated equibiaxial tensile data were generated. The material parameters (c, μ_a, λ_{ab}) that best fit the constitutive model (Equation 2) to this simulated data were then calculated (Table 1).

To investigate the differences the constitutive model of skin has on landmark displacements during facial expressions, we substituted the constitutive model of Equation 1 in place of the Fung model (Equation 2) for the outer layer of elements representing skin. The material parameters of all soft tissue elements were those specified by Nazari et al. (2010) (Table 1). The open-mouthed smile was simulated and the results compared with the corresponding simulation using the Fung model for the skin layer.

Imposition of an in vivo skin tension

All the reference coordinates of the soft tissue nodes are scaled before the first step in the FE analysis (designated here as a Tension Scaling Factor (TSF)). During the first step, the inside nodes of the soft tissue mesh are displaced from their scaled coordinate positions to their original reference coordinates positions. This results in a pre-stress field in the soft tissue representing the *in vivo* tension in human skin. The pre-stress level can be changed by varying the TSF for nodal coordinates.

Next, reaction forces on most inner surface face nodes, which do not have any displacement boundary conditions for subsequent steps in the analysis, are linearly reduced to zero during a

time period. This is a more stable procedure than suddenly releasing these nodes.

Facial Expression Analyses

Various facial expressions were simulated using the model. The expressions included wide opening of the mouth, closed-mouth smile, open-mouth smile, pursing of the lips, and lips turned downwards.

Opening the mouth wide was simulated by activating the upper and lower heads of the lateral pterygoid muscles and the anterior and posterior belly of the digastric muscle (Stavness et al. 2011). The other expressions were simulated by activating the appropriate facial muscles (Table 3). For wide opening of the mouth, and the closed-mouth smile, the changes in direction of the maximum principal tension at points on the facial surface were calculated. For all expressions, the displacements of facial landmarks were calculated (Figure 4). The landmarks correspond to points on the face used as references in facial skin experiments (Coulson et al. 2000, Coulson et al. 2002, Giovanoli et al. 2003, Houstis and Kiliaridis 2009, Schimmel et al. 2010, Sforza et al. 2010, Verze et al. 2011). The distances between certain pairs of landmarks for each expression were also calculated. Facial landmark displacements were not calculated for the opening of the mouth as there was no experimental data to compare the simulation to.

Effects of Skin Material Parameters

The effects of aging skin on the landmark displacement for various facial expressions were also investigated. In order to simulate skin of different ages, the *in vivo* tension in the skin model was varied by varying the Tension Scaling Factor and the stiffness of the skin layer was also varied (Flynn and McCormack 2008, Flynn and McCormack 2009) (see Table 1).

Results

Displacing the inside nodes of the soft tissue mesh from their scaled positions to the resting volunteer specific positions resulted in an *in vivo* tension field within the soft tissue layers. The directions of the maximum principal tensions at different points on the skin surface were similar to the RSTLs of Borges (1984) (Figure 5(a)).

When the mouth was wide open (Figure 6(a)), the orientations of the principal tension lines changed (Figure 5(b)). The areas around the chin and anterior mandible experienced the largest change in orientation of up to 90^{o}, while regions around the temples experienced little or no change in orientation. The mean rotation of principal tension directions on the face was 18^{o}. The distance between the upper and lower central incisors was 40 mm when the mouth was wide open.

When open-mouth smiling (Figure 6(b)), the mean rotation of the principal tension directions on the face was 25^{o} (Figure 5(c)). Large rotations up to 90^{o} occurred around the cheek regions, while areas around the temple and nasal regions experienced smaller rotations.

For the open-mouth smile (Figure 6(b)), the range of facial landmark displacements was between 3.5 mm and 12 mm for 'normal' skin (Figure 7(a)). Largest displacements were calculated for the right mouth corner, while the chin landmark (PG) displaced the least amount. The distance between the left and right mouth corners (RMC-LMC) increased by 18% for 'normal' skin (Figure 8(a)), while the distance between the ear and mouth corner (RC-RMC) decreased by 18%. The distance between the upper and lower lip (PH-SL) increased by almost 30%. For a closed-mouth smile (Figure 6(c)), the right mouth (RMC) corner also experienced the greatest displacement of 10.7 mm for 'normal' skin (Figure 7(b)). The PG displacement was much greater than the displacement for an open-mouth smile. For lip pursing (Figure 6(d)), the

lip area landmarks including the mouth corner, upper lip, and lower lip, experienced the largest displacements of up to 14 mm for ‘normal’ skin (Figure 7(c)). The distance between the mouth corners reduced by 25% for ‘normal’ skin (Figure 8(b)). When the lips are turned down (Figure 6(e)), the mouth corners are displaced the most at about 11 mm for ‘normal’ skin (Figure 7(d)).

For open and closed-mouth smiles, increasing the stiffness of the skin layer resulted in smaller landmark displacements (Figure 7(a) and Figure 7(b)). There was also a general decrease in the change in distance between landmarks with an increasing stiffness (Figure 8(a)). For pursing and turning down of the lips, there were also smaller landmark displacements with increasing skin stiffness (Figure 7(c) and Figure 7(d)). There were exceptions to this trend including the central upper-lip displacement (PH) when pursing the lips, and the central upper and lower-lip displacements (PH, SL) when turning the lips down.

Increasing the *in vivo* tension had a varying effect on landmark displacements (Figure 9). For example, the central upper-lip displacement (PH) increases with increasing tension for the smiling expressions but decreases with increasing tension when the lips are pursed and turned down. It also had a varying effect on the change in distance between landmarks (Figure 10).

Substituting an isotropic model using the Mooney-Rivlin parameter values of Nazari et al. (2010) in place of the orthotropic Fung model resulted in smaller landmark displacements for an open-mouth smile (Figure 11).

Discussion

Simulating the mechanical behaviour of the human face is a challenging endeavour. There are many different complex interactions and behaviours, such as contact between hard and soft tissues, the relative movement between tissues, jaw motion, and the mechanical properties of the various soft tissue layers. The benefits of capturing certain key aspects of these behaviours are

manifold, including improved maxillofacial surgery planning (Cavicchi et al. 2009, Sharifi et al. 2008), better understanding of speech production (Bucki et al. 2010), and superior animation quality (Zhang et al. 2006).

A finite element model of the face has been proposed, where the anisotropic and multi-layer characteristics of the skin and hypodermis have been represented. A method for including the *in vivo* tension natural to human skin has also been proposed. To the best of the authors' knowledge, this is the first finite element face model that includes the *in vivo* tension and anisotropic properties for facial skin. This represents a significant development over existing face models, which ignore these characteristics (Barbarino et al. 2009, Beldie et al. 2010, Nazari et al. 2010).

The resting state of the facial skin in the proposed model contains a tension field, whose maximum principal directions at points on the face are similar to the RSTL pattern observed by Borges (1984). Upon facial expression, such as wide opening of the mouth or smiling, these principal directions rotated. This behaviour is in agreement with Bush et al (2007), who observed the rotation of patients' elliptical wound axes when producing standardised facial expressions. For wide opening of the mouth, the principal tension directions predicted by the model agree with experimental observations in the upper-lip, chin, anterior mandibular, temple, and some cheek areas (Figure 5(b)). Similarly, for smiling, directions predicted by the model agree with experimental observations in the lower-lip, upper-lip, chin, and some cheek areas (Figure 5(c)). Bush et al. (2007) observed orientations of wound axes at the same point in different volunteers, which differed by up to 90^{o}, demonstrating that there is possibly a large inter-volunteer variability in the *in vivo* tension field. Bush et al. (2007) calculated a median rotation of 30^{o} in the long axis of wounds for different facial expressions. This compares to a mean rotation of

principal tension directions of 17° for wide opening of the mouth and 25° for smiling. The lower rotation predicted for wide mouth opening may partially be explained by the amount the mouth was opened. The lower to upper central incisor distance was 40 mm, whereas average mouth openings of 52 mm with maximum openings of 67 mm have been reported (Mezitis et al. 1989). The rotation of the tension field during a facial expression may affect the appearance of a healed facial wound and should be taken into account when planning an incision (Bush et al. 2007). For this reason, the inclusion of the *in vivo* tension in the face model is an important and significant development and an improvement over previously proposed models, which do not include it.

Modelling facial wounds and scars and examining their effect on facial expressions would be an interesting extension of this study. Skin anisotropy and *in vivo* tension are known to be important factors in the ability of a wound to heal with minimal scarring and return to full function (Borges 1989, Cerda 2005, Flynn and MacCormack 2008). Due to their higher collagen content, scar material is stiffer than the surrounding normal tissue and so would have an influence on facial skin mechanics (Dunn et al. 1985). Therefore, investigating the ability of the proposed model to quantify the effects of wounds and scars on facial skin function would represent a significant advancement in face modelling.

The landmark displacements predicted by the proposed model for different expressions are in good agreement with displacements reported in the literature. For the open-mouth smile, the predicted mouth corner displacement is within the range of displacements measured by Coulson et al. (2000), Sforza et al. (2010), and Giovanoli et al. (2003). There is also good agreement for other landmarks, which have a large range of displacement, such as PG, PH, RAN, RML, RMU, and SL (Figure 7(a)). The predicted changes in distances between certain landmarks for an open-mouth smile agree well with the changes measured by Houstis and

Killiardis (2009) and Schimmel et al. (2010) (Figure 8(a)). The sign of the change agrees for all predicted and measured distances. All predicted distance changes are within a standard deviation of the measured mean distance change except for the change in the subnasal-upper lip distance (SN-PH). Further adjustment of muscle activations may reduce this discrepancy. There is excellent agreement between the closed-mouth smile mouth corner and upper lip displacements predicted by the model and the displacements measured by Giovanoli et al. (2003) (Figure 7(b)). However, the lower lip displacement (RML) is higher than the corresponding experimental measurement. Giovanoli et al. (2003) did not report on the variance of the experimental measurements so we do not know whether the predicted RML displacement lay within the range of their 24 samples. The mouth corner displacement (RMC) when pursing the lips is within a standard deviation of the mean displacement predicted by Coulson et al. (2000). While the predicted magnitude of change in distances between landmarks for lip pursing are within a standard deviation of the corresponding experimental measurements of Houstis and Killiardis (2009), their signs do not agree (Figure 8(b)). For example, Houstis and Killiardis (2009) measured an increase in the distance between the upper and lower lip but the model predicted a decrease in this same distance. The reason for this may be that for the experiment rest state, the lips were together, whereas for the model, the lips were parted. The displacement of the mouth corners (RMC) when turning down the lips agrees with the mean of the mouth corner displacement measured by Coulson et al. (2000). Overall, it has been demonstrated that in addition to simulating realistic facial expressions, the proposed model can also accurately simulate the displacement of landmarks for these expressions.

The proposed model has demonstrated that the change in properties associated with skin aging has a significant effect on facial deformations. As skin ages, it undergoes several

biological changes including changes in stiffness (Batisse et al. 2002, Wulf et al. 2004), and a loss in its natural tension or tone due to due in part to the thinning of the hypodermis, laxity in the retaining ligaments, and skeletal resorption (Albert et al. 2007, Quatresooz et al. 2006). Sforza et al. (2010) observed larger landmark displacements for maximum smile expressions in older volunteers but smaller landmark displacements for free smiles in older volunteers. It is noted that these results were not statistically significant. Giovanoli et al. (2003) reported a general increase in landmark displacements with increasing age for various facial expressions. The proposed model predicted that as the stiffness of the skin increased, the landmark displacements decreased and the change in distance between landmarks decreased (Figure 7 and Figure 8). The effect of changing tension on landmark displacement is more varied. For each facial expression, some landmark displacements increased with increasing *in vivo* tension, some displacements decreased, while others showed an initial increase followed by a decrease (Figure 9). The change in distance between landmarks also showed a varying relationship with the *in vivo* tension (Figure 10).

Simulating an aging face by only changes in skin stiffness and *in vivo* tension is a simplification of the reality. Other factors of aging, including changes in skin thickness, bone resorption, and facial muscle changes have not been considered in the model. However, it is informative to investigate certain changes in isolation to observe their effect.

The results from the model have also demonstrated the effect of the material model on the results (Figure 11). There were significant differences in the landmark displacements during an open-mouth smile when the orthotropic Fung model was substituted for the isotropic Mooney-Rivlin model used in Nazari et al. (2010). It is important to use appropriate constitutive

models and volunteer-specific material parameters in order to accurately simulate the mechanical behaviour of a volunteer's face.

There are several simplifying assumptions in the finite element model of the face in this study. The nature of the connection between the skin and hypodermis needs to be established, as well as the connection between the hypodermis and bony structures. The material parameters for the facial muscles also need to be determined from experimental measurements. The current passive muscle parameters are based on properties of the biceps brachii (Blemker et al. 2005). More accurate facial muscle properties would likely result in changes to the muscle activations needed to generate each facial expression. Human skin exhibits viscoelastic behaviour (Flynn et al. 2011), which has been ignored in the proposed model. Indeed, the material parameters of the skin layer and the applied *in vivo* tensions are based on forearm skin experimental data (Evans and Holt 2009, Flynn et al. 2011). The model would be improved if material parameters specific to facial skin were used in the constitutive equation. There is a relative dearth of experimental data in the literature that characterises the anisotropic behaviour of facial skin. Most experimental protocols are unable to determine the anisotropic behaviour (Barbarino et al. 2011, Couturaud et al. 1995, Malm et al. 1995, Tsukahara et al. 2004) while those that do ignore the non-linear stress-strain characteristics of skin under large deformations (Ohshima, 2011). Recently, *in vivo* experiments on human facial skin using a protocol similar to Flynn et al. (2011) have been carried out (to be published). The anisotropic and viscoelastic mechanical response of the facial skin has been characterised and appropriate material parameters determined. Initial analyses indicate that the stiffness of facial skin varies according to regions of the face. Comparing with results of Flynn et al. (2011), the central cheek, lip, and zygomatic regions are less stiff than forearm skin; the forehead region has a similar stiffness, while the mandible region

is stiffer than forearm skin. Of course, the mechanical properties of skin vary widely according to individual and site (Ridge and Wright, 1966). As the mechanical response of forearm skin is within the range of responses measured in facial skin, the material parameters are appropriate to use as a first step in the development of an anisotropic face model. Future developments of the model will include the use of volunteer-specific geometries and material parameters specific to different regions of the face.

Acknowledgements

CF was supported by a fellowship from the Michael Smith Foundation for Health Research.

Appendix: Facial muscle modelling

The total Cauchy stress of the muscle fibre with a reference direction $\mathbf{a}_0$ is given by (Weiss et al. 1996)

$$\sigma_{fibre} = \frac{2W_4\bar{\lambda}_f^2}{J}\left(\mathbf{a}\otimes\mathbf{a} - \frac{1}{3}\mathbf{I}\right) \tag{4}$$

where $\mathbf{a} = \mathbf{F}\mathbf{a}_0 / |\mathbf{F}\mathbf{a}_0|$ is the deformed fibre direction, $\otimes$ is the tensor product operator, $\mathbf{I}$ is the second order identity tensor. $\bar{\lambda}_f$ is the distortional fibre stretch given by

$$\bar{\lambda}_f = J^{-1/3}|\mathbf{F}\mathbf{a}_0| \tag{5}$$

Also,

$$W_4 = \frac{f_p^{fibre}\left(\bar{\lambda}_f\right) + \alpha\sigma_{\max}}{2\bar{\lambda}_f} \tag{6}$$

where α is the activation level of the active fibre stress, $\sigma_{\max}$ is the maximum active stress within the muscle fibre, and $f_p^{fibre}\left(\bar{\lambda}_f\right)$ is the normalised passive force in the muscle fibre, which is given

by (Blemker et al. 2005)

$$f_p^{fibre}\left(\bar{\lambda}_f\right)=\begin{cases}0, \bar{\lambda}_f<1\\ P_1\left(e^{P_2\left(\bar{\lambda}_f-1\right)}-1\right), 1\le\bar{\lambda}_f<\lambda^*\\ P_3\bar{\lambda}_f+P_4, \bar{\lambda}_f\ge\lambda^*\end{cases} \quad (7)$$

P_1 is an exponential stress coefficient, P_2 is an uncrimping factor, and λ^* is the stretch at which $f_p^{fibre}\left(\bar{\lambda}_f\right)$ becomes linear. P_3 and P_4 are defined so that $f_p^{fibre}\left(\bar{\lambda}_f\right)$ is C0 and C1 continuous at $\bar{\lambda}_f=\lambda^*$. The total stress response of the facial muscle is added to the stress response of the soft tissue. The values for P_1, P_2, λ^*, and σ_{max} are given in Table 4. The simulated uniaxial stress-stretch behaviour of muscle fibres for the activations used for the facial expressions is shown in Figure 12.

References

Albert AM, Ricanek K, Jr., Patterson E. 2007. A review of the literature on the aging adult skull and face: Implications for forensic science research and applications. Forensic Sci Int 172(1):1-9.

Ateshian GA and Costa KD. 2009. A frame-invariant formulation of fung elasticity. J Biomech 42(6):781-5.

Barbarino GG, Jabareen M, Trzewik J, Nkengne A, Stamatas G, Mazza E. 2009. Development and validation of a three-dimensional finite element model of the face. J Biomech Eng 131(4):041006-11.

Barbarino GG, Jabareen M, Mazza E. 2011. Experimental and numerical study on the mechanical behavior of the superficial layers of the face. Skin Research and Technology 17(4):434-44.

Batisse D, Bazin R, Baldeweck T, Querleux B, Lévêque J. 2002. Influence of age on the wrinkling capacities of skin. Skin Res Technol 8(3):148-54.

Beldie L, Walker B, Lu Y, Richmond S, Middleton J. 2010. Finite element modelling of maxillofacial surgery and facial expressions - a preliminary study. Int J Med Robot Comput Assist Surg 6(4):422-30.

Bellamy K, Limbert G, Waters MG, Middleton J. 2003. An elastomeric material for facial prostheses: Synthesis, experimental and numerical testing aspects. Biomaterials 24(27):5061-6.

Blemker SS, Pinsky PM, Delp SL. 2005. A 3D model of muscle reveals the causes of nonuniform strains in the biceps brachii. J Biomech 38(4):657-65.

Borges A. 1984. Relaxed skin tension lines (rstl) versus other skin lines. Plast Reconstr Surg 73(1):144-50.

Borges AF. 1989. Relaxed skin tension lines. Dermatologic Clinics 7(1):169-77.

Bucki M, Nazari MA, Payan Y. 2010. Finite element speaker-specific face model generation for the study of speech production. Comput Methods Biomech Biomed Engin 13(4):459-67.

Bush J, Ferguson MWJ, Mason T, McGrouther G. 2007. The dynamic rotation of langer's lines on facial expression. Journal of Plastic, Reconstructive & Aesthetic Surgery 60(4):393-9.

Cavicchi A, Gambarotta L, Massabò R. 2009. Computational modeling of reconstructive surgery: The effects of the natural tension on skin wrinkling. Finite Elements in Analysis and Design 45(8-9):519-29.

Cerda E. 2005. Mechanics of scars. J Biomech 38(8):1598-603.

Chabanas M, Luboz V, Payan Y. 2003. Patient specific finite element model of the face soft tissues for computer-assisted maxillofacial surgery. Med Image Anal 7(2):131-51.

Claes P, Vandermeulen D, De Greef S, Willems G, Clement JG, Suetens P. 2010. Computerized craniofacial reconstruction: Conceptual framework and review. Forensic Sci Int 201(1-3):138-45.

Coulson S, Croxson G, Gilleard W. 2002. Three-dimensional quantification of the symmetry of normal facial movement. Otology & Neurotology 23(6):999-1002.

Coulson S, Croxson G, Gilleard W. 2000. Quantification of the three-dimensional displacement of normal facial movement. Annals of Otology Rhinology and Laryngology 109(5):478-83.

Couturaud V, Coutable J, Khaiat A. 1995. Skin biomechanical properties: In vivo evaluation of influence of age and body site by a non-invasive method. Skin Research and Technology 1(2):68-73.

Domaracki M and Stephan C. 2006. Facial soft tissue thicknesses in australian adult cadavers. J Forensic Sci 51(1):5-10.

Dunn MG, Silver FH, Swann DA. 1985. Mechanical analysis of hypertrophic scar tissue: Structural basis for apparent increased rigidity. Journal of Investigative Dermatology 84(1):9-13.

Evans SL and Holt CA. 2009. Measuring the mechanical properties of human skin in vivo using digital image correlation and finite element modelling. Journal of Strain Analysis for Engineering Design 44(5):337-45.

Flynn C, Taberner A, Nielsen P. 2011. Modeling the mechanical response of *in vivo* human skin under a rich set of deformations. Ann Biomed Eng 39(7):1935-46.

Flynn C and McCormack BAO. 2009. Simulating the wrinkling and aging of skin with a multi-layer finite element model. J Biomech 43(3):442-8.

Flynn C and McCormack BAO. 2008. Finite element modelling of forearm skin wrinkling. Skin Res Technol 14(3):261-9.

Flynn C, Taberner A, Nielsen P. 2011. Measurement of the force–displacement response of in vivo human skin under a rich set of deformations. Med Eng Phys 33(5):610-9.

Furnas D. 1989. The retaining ligaments of the cheek. Plast Reconstr Surg 83(1):11-6.

Giovanoli P, Tzou C-J, Ploner M, Frey M. 2003. Three-dimensional video-analysis of facial movements in healthy volunteers. Br J Plast Surg 56(7):644-52.

Gladilin E, Zachow S, Deuflhard P, Hege HC. 2004. Anatomy- and physics-based facial animation for craniofacial surgery simulations. Med Biol Eng Comput 42(2):167-70.

Ha R, Nojima K, Adams W, Brown S. 2005. Analysis of facial skin thickness: Defining the relative thickness index. Plast Reconstr Surg 115(6):1769-73.

Hannam AG. 2011. Current computational modelling trends in craniomandibular biomechanics and their clinical implications. J Oral Rehabil 38(3):217-34.

Houstis O and Kiliaridis S. 2009. Gender and age differences in facial expressions. Eur J Orthod 31(5):459-66.

Kim H, Juergens P, Weber S, Nolte L, Reyes M. 2010. A new soft-tissue simulation strategy for cranio-maxillofacial surgery using facial muscle template model. Progress in Biophysics & Molecular Biology 103(2-3):284-91.

Lee Y and Hwang K. 2002. Skin thickness of korean adults. Surgical and Radiologic Anatomy 24(3-4):183-9.

Malm M, Samman M, Serup J. 1995. In vivo skin elasticity of 22 anatomical sites. Skin Research and Technology 1(2):61-7.

Manheim M, Listi G, Barsley R, Musselman R, Barrow N, Ubelaker D. 2000. In vivo facial tissue depth measurements for children and adults. J Forensic Sci 45(1):48-60.

Mezitis M, Rallis G, Zachariades N. 1989. The normal range of mouth opening. J Oral Maxillofac Surg 47(10):1028-9.

Mollemans W, Schutyser F, Nadjmi N, Maes F, Suetens P. 2007. Predicting soft tissue deformations for a maxillofacial surgery planning system: From computational strategies to a complete clinical validation. Med Image Anal 11(3):282-301.

Nazari MA, Perrier P, Chabanas M, Payan Y. 2011. Shaping by stiffening: A modeling study for lips. Motor Control 15(1):141-68.

Nazari MA, Perrier P, Chabanas M, Payan Y. 2010. Simulation of dynamic orofacial movements using a constitutive law varying with muscle activation. Comput Methods Biomech Biomed Engin 13(4):469-82.

Ohshima H, Tada A, Kanamaru A, Akamatsu H, Sakai Y, Itoh M, Kanto H. 2011. Relevance of the directionality of skin elasticity to aging and sagging of the face. Skin Res Technol 17(1):101-7.Quatresooz P, Thirion L, Pierard-Franchimont C, Pierard GE. 2006. The riddle of genuine skin microrelief and wrinkles. International Journal of Cosmetic Science 28(6):389-95.

Schimmel M, Christou P, Houstis O, Herrmann FR, Kiliaridis S, Mueller F. 2010. Distances between facial landmarks can be measured accurately with a new digital 3-dimensional video system RID F-5694-2011 RID B-6710-2011. American Journal of Orthodontics and Dentofacial Orthopedics 137(5):580.e1.

Sforza C, Mapelli A, Galante D, Moriconi S, Ibba TM, Ferraro L, Ferrario VF. 2010. The effect of age and sex on facial mimicry: A three-dimensional study in healthy adults. Int J Oral Maxillofac Surg 39(10):990-9.

Sharifi A, Jones R, Ayoub A, Moos K, Walker F, Khambay B, McHugh S. 2008. How accurate is model planning for orthognathic surgery? Int J Oral Maxillofac Surg 37(12):1089-93.

Stavness I, Lloyd JE, Payan Y, Fels S. 2011. Coupled hard–soft tissue simulation with contact and constraints applied to jaw–tongue–hyoid dynamics. Int J Numer Meth Biomed Engng 27(3):367-90.

Tsukahara K, Moriwaki S, Hotta M, Fujimura T, Kitahara T. 2004. A study of diurnal variation in wrinkles on the human face. Archives of Dermatological Research 296(4):169-74.

Verze L, Nasi A, Quaranta F, Vasino V, Prini V, Ramieri G. 2011. Quantification of facial movements by surface laser scanning. J Craniofac Surg 22(1):60-5.

Virgin FW, Iseli TA, Iseli CE, Sunde J, Carroll WR, Magnuson JS, Rosenthal EL. 2010. Functional outcomes of fibula and osteocutaneous forearm free flap reconstruction for segmental mandibular defects. Laryngoscope 120(4):663-7.

Weiss J, Maker B, Govindjee S. 1996. Finite element implementation of incompressible, transversely isotropic hyperelasticity RID B-6886-2008. Comput Methods Appl Mech Eng 135(1-2):107-28.

Wilkes GL, Brown IA, Wildnauer RH. 1973. The biomechanical properties of skin. CRC Cr Rev Biotechn 1(4):453-95.

Ridge MD, Wright V, 1966. Mechanical properties of skin: a bioengineering study of skin structure. Journal of applied physiology 21(5):1602-1606.

Wulf HC, Sandby-Møller J, Kobayasi T, Gniadecki R. 2004. Skin aging and natural photoprotection. Micron 35(3):185-91.

Zhang Q, Liu Z, Gaining Q, Terzopoulos D, Shum HY. 2006. Geometry-driven photorealistic facial expression synthesis. IEEE Transactions on Visualization and Computer Graphics 12(1):48-60.

Zhang Y, Prakash E, Sung E. 2004. Face alive. Journal of Visual Languages and Computing 15(2):125-60.

Figure Legends

Figure 1. Finite element model of the face

Figure 2. Orofacial muscles including the element muscle fibres

Figure 3. (a) Relaxed skin tension lines traced on the surface of the face; (b) Relaxed skin tension line direction assigned to elements closest to it

Figure 4. Facial landmarks: RC – Right inner canthus; ROR – Right orbital; RAN – Right ala of the nose; SN - Subnasale; RMU - Right midlateral point of upper lip; PH - Philtrum; RMC – Right mouth corner; LMC – Left mouth corner; RML – Right midlateral point of lower lip; SL - Sublabiale; PG - Pogonion

Figure 5. Vector field of maximum principal tension in the skin: (a) At rest; (b) Mouth wide open; (c) Open-mouth smiling. For comparison with experimental data, results for (b) and (c) are shown on the face at rest – see Figure 6 for the expressions. For each figure, blue lines represent the tension field in the face model at rest; red lines represent the tension field in the face model during the facial expression; yellow lines represent the orientation of long axes of wounds (from Bush et al (Bush, Ferguson et al. 2007))

Figure 6. Facial Expressions: (a) Wide open mouth; (b) Open-mouth smile; (c) Closed-mouth smile; (d) Lip pursing; (e) Lips turned down

Figure 7. Landmark displacements for different skin-types after (a) an open-mouth smile; (b) a closed-mouth smile; (c) lip pursing; (d) lips turned down. Material parameters for different skin-types are specified in Table 1.

Figure 8. Percentage change of distance between landmarks for different skin-types after (a) an open-mouth smile; (b) lip pursing. Material parameters for different skin-types are specified in Table 1.

Figure 9. Landmark displacements for facial skin with different *in vivo* tensions after (a) an open-mouth smile; (b) a closed-mouth smile; (c) lip pursing; (d) lips turned down.

Figure 10. Percentage change of distance between landmarks for facial skin with different *in vivo* tensions (a) an open-mouth smile; (b) lip pursing.

Figure 11. Comparing landmark displacements during an open-mouth smile using the Fung and Mooney-Rivlin skin models. Material parameters for the skin models are specified in Table 1.

Figure 12. Stress-stretch response of muscle fibre for different activations α used in facial expressions (see Table 3). The curve for α=0 gives the passive response of the muscle fibre.

Table 1. Material parameters for different skin-types; TSF – Tension Scale Factor

Skin Type	c (kPa)	μ_1 (kPa)	μ_2 (kPa)	μ_3 (kPa)	λ_{11} (kPa)	$\lambda_{22}, \lambda_{33}, \lambda_{12}, \lambda_{23}, \lambda_{31}$ (kPa)	κ (kPa)	TSF
Normal	21.3	17.8	5.9	5.9	1.0	1.0	250.0	1.10
Stiff	42.6	35.6	11.8	11.8	11.8	2.0	250.0	1.05
Soft	10.7	8.9	3.0	3.0	0.5	0.5	250.0	1.15

	C_{10} (kPa)	C_{20} (kPa)	κ (kPa)
Money-Rivlin skin (Nazari et al. 2010)	2.5	1.175	250.0

Table 2. Material parameters of Hypodermis

C_{10} (kPa)	C_{20} (kPa)	D (kPa)
0.4	1.4	50

Table 3. Muscles activated for each expression

Muscle	Activation Level, α			
	Closed-Mouth Smile	Open-Mouth Smile	Lips Turned Down	Pursed Lips
Zygomaticus (ZYG)	0.2	0.5	0.0	0.0
Levator Labii Superioris Alaeque Nasi (LLSAN)	0.1	0.5	0.0	0.0
Levator Anguli Oris (LAO)	0.1	0.5	0.0	0.0
Risorius (RIS)	0.2	0.6	0.6	0.0
Depressor Labii Inferioris (DLI)	0.0	0.5	0.0	0.0
Depressor Anguli Oris (DAO)	0.0	0.5	1.0	0.0
Mentalis (MENT)	0.0	0.0	0.15	0.0
Orbicularis Oris Peripheralis (OOP)	0.0	0.0	0.0	0.5
Orbicularis Oris Marginalis (OOM)	0.0	0.0	0.0	0.1
Buccinator (BUC)	0.0	0.0	0.0	0.4

Table 4. Material parameters of facial muscles

λ^*	σ_{max} (kPa)	P_1	P_2
1.4	100	0.05	6.6

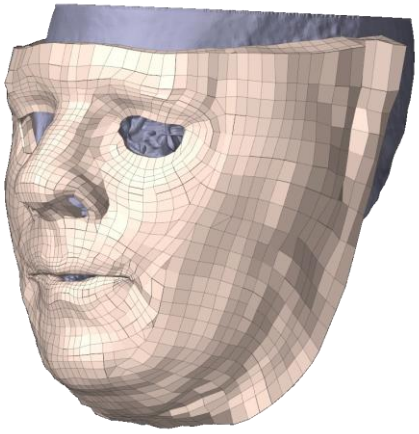

Figure 1

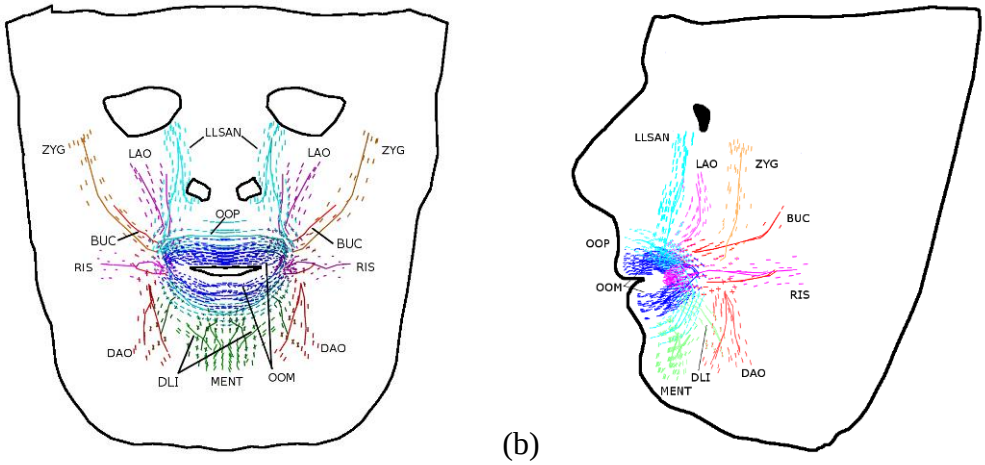

(a) (b)

Figure 2

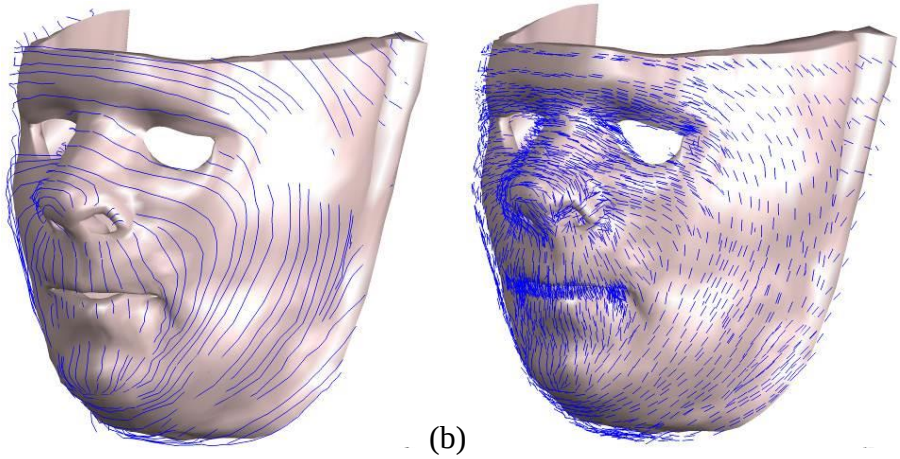

(a) (b)

Figure 3

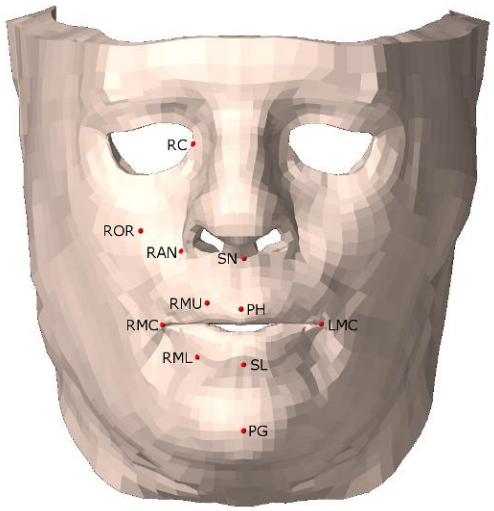

Figure 4

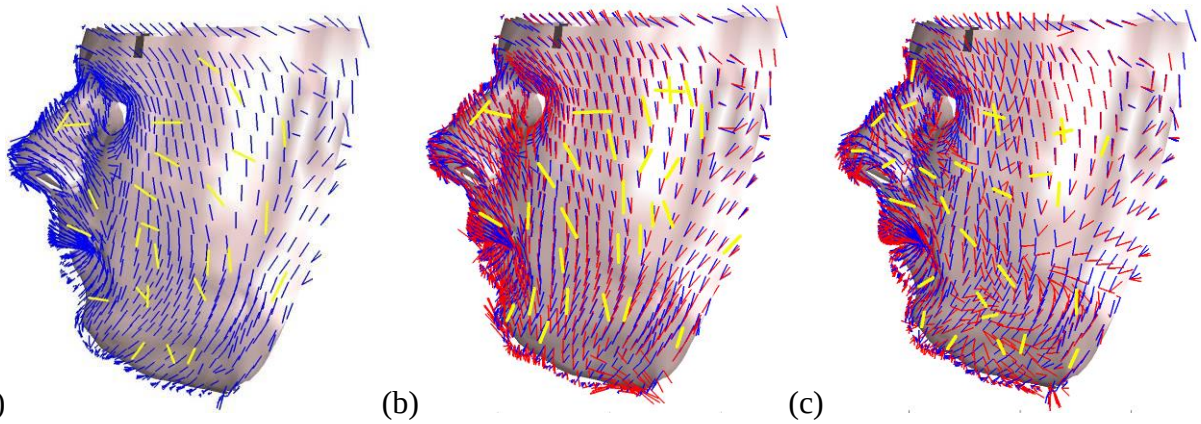

(a) (b) (c)

Figure 5

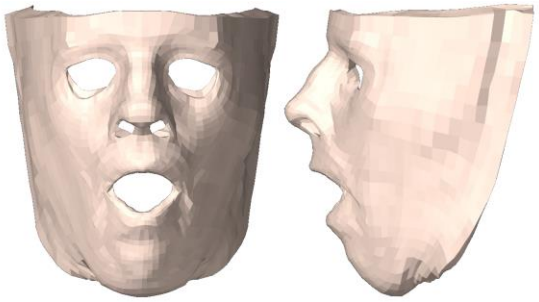

(a)

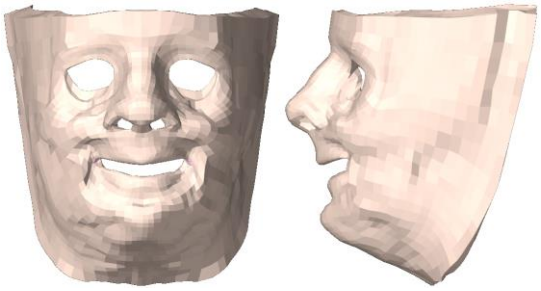

(b)

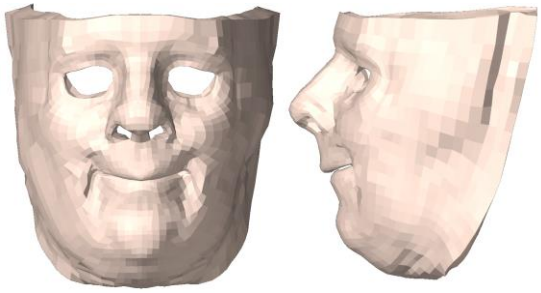

(c)

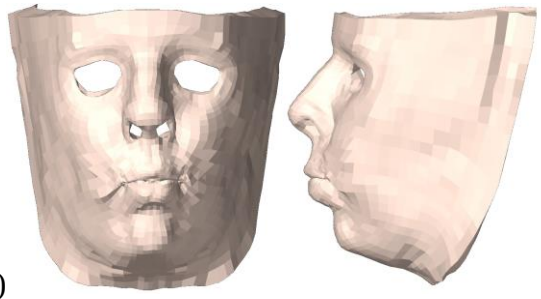

(d)

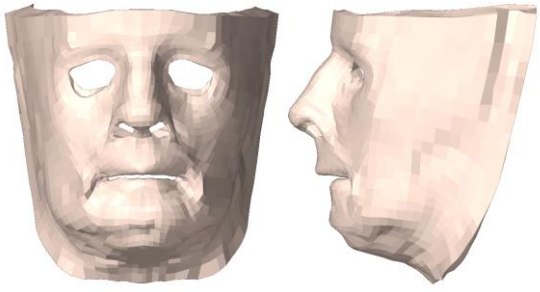

(d)

Figure 6

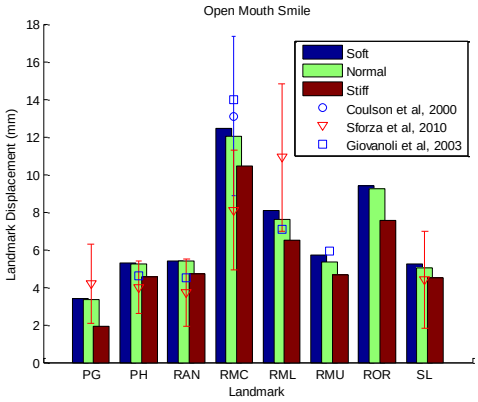

(a)

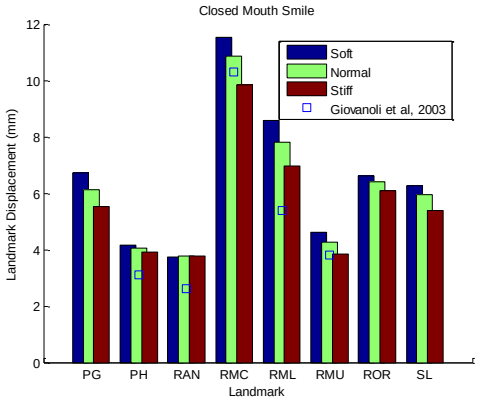

(b)

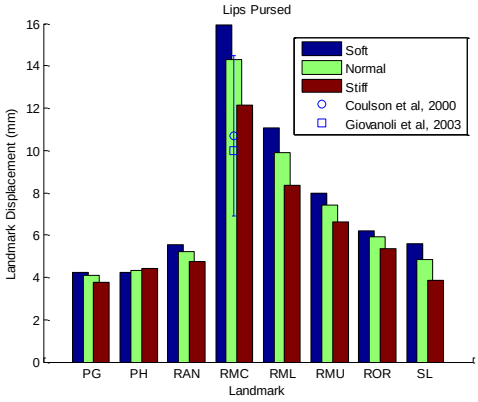

(c)

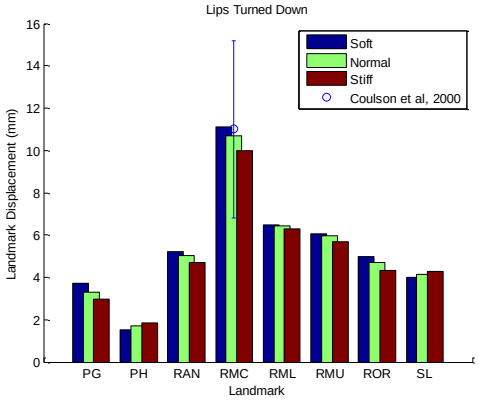

(d)

Figure 7

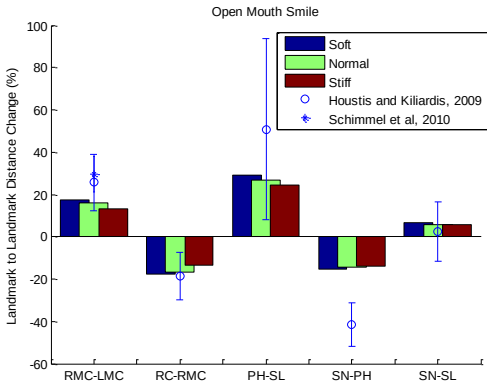

(a)

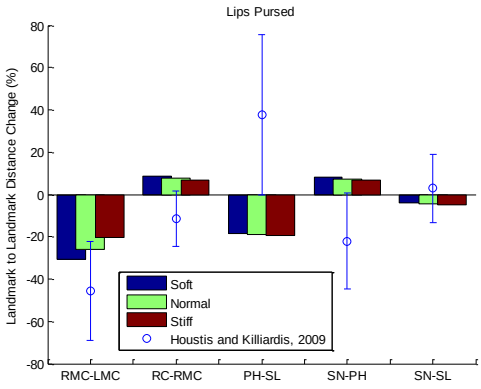

(b)

Figure 8

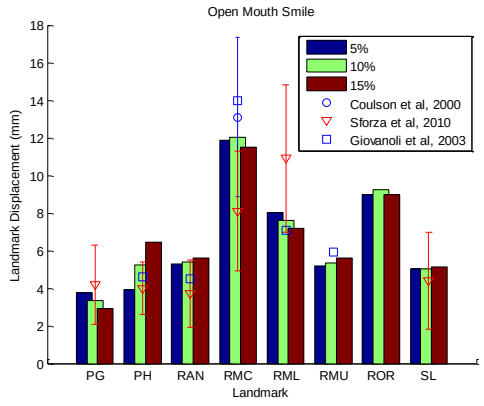

(a)

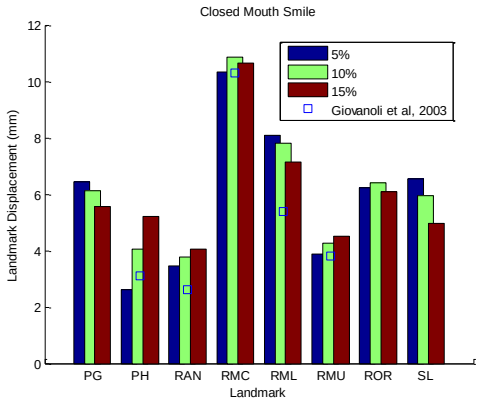

(b)

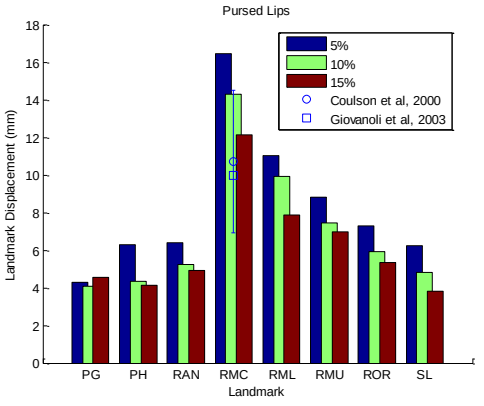

(c)

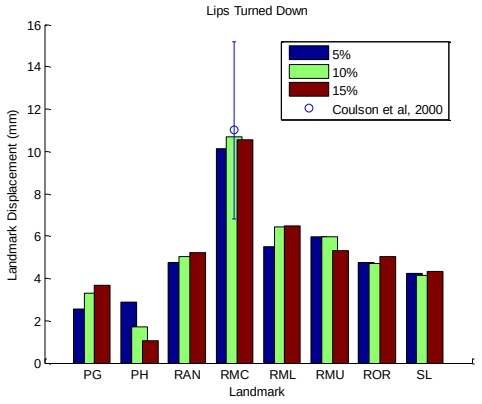

(d)

Figure 9

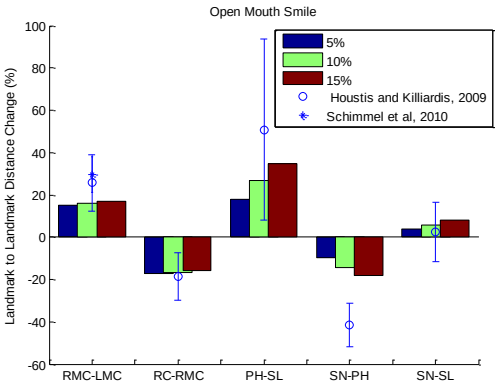

(a)

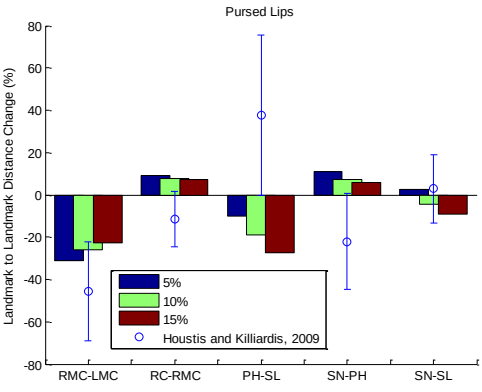

(b)

Figure 10

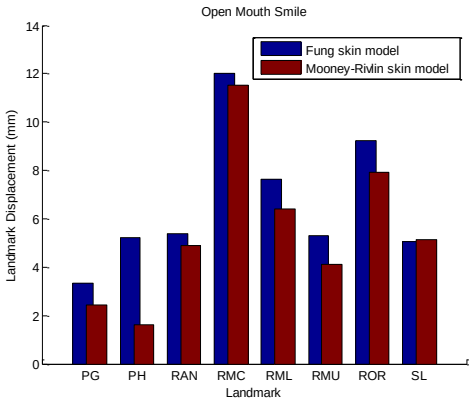

Figure 11

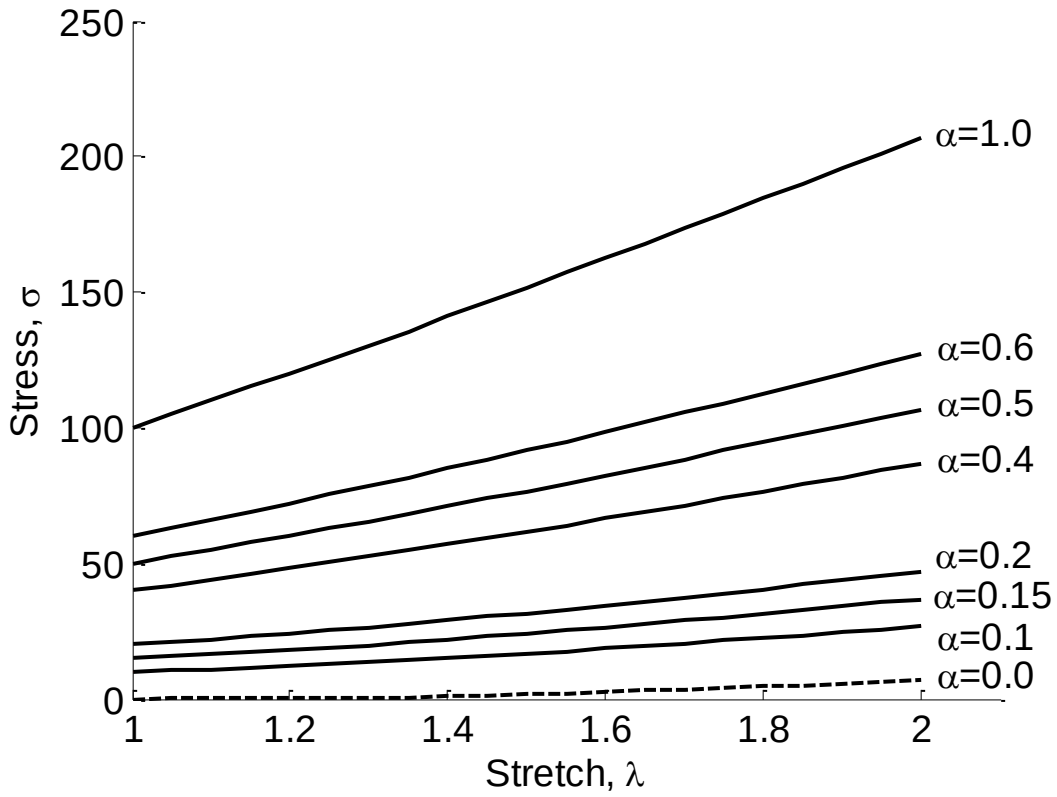

Figure 12